

# Analytic Structure of the SCFT Energy Functional of Multicomponent Block Copolymers

Kai Jiang,<sup>1,2, a)</sup> Weiquan Xu,<sup>2</sup> and Pingwen Zhang<sup>2, b)</sup>

<sup>1)</sup>*Hunan Key Laboratory for Computation and Simulation in Science and Engineering, School of Mathematics and Computational Science, Xiangtan University, Hunan, P.R. China, 411105*

<sup>2)</sup>*LMAM, CAPT and School of Mathematical Sciences, Peking University, Beijing 100871, P.R. China*

(Dated: 15 November 2018)

This paper concerns the analytic structure of the self-consistent field theory (SCFT) energy functional of multicomponent block copolymer systems which contain more than two chemically distinct blocks. The SCFT has enjoyed considered success and wide usage in investigation of the complex phase behavior of block copolymers. It is well-known that the physical solutions of the SCFT equations are saddle points, however, the analytic structure of the SCFT energy functional has received little attention over the years. A recent work by Fredrickson and collaborators [see the monograph by Fredrickson, *The Equilibrium Theory of Inhomogeneous Polymers*, (2006), pp. 203–209] has analysed the mathematical structure of the field energy functional for polymeric systems, and clarified the index-1 saddle point nature of the problem produced by the incompressibility constraint. In this paper, our goals are to draw further attention to multicomponent block copolymers utilizing the Hubbard-Stratonovich transformation used by Fredrickson and co-workers. We first show that the saddle point character of the SCFT energy functional of multicomponent block copolymer systems may be high index, not only produced by the incompressibility constraint, but also by the Flory-Huggins interaction parameters. Our analysis will be beneficial to many theoretical studies, such as the nucleation theory of ordered phases, the mesoscopic dynamics. As an application, we then utilize the discovery to develop the gradient-based iterative schemes to solve the SCFT equations, and illustrate its performance through several numerical experiments taking *ABC* star triblock copolymers as an example.

---

<sup>a)</sup>Electronic mail: kaijiang@xtu.edu.cn

<sup>b)</sup>Electronic mail: pzhang@pku.edu.cn

## I. INTRODUCTION

Due to the efforts of a large number of researchers, it has been well-established that the self-consistent field theory (SCFT) of polymers provides a powerful theoretical framework for the study of inhomogeneous polymeric systems in general and the self-assembly behavior of block copolymers in particular<sup>1-3</sup>. For a given block copolymer system, the SCFT can be efficiently describe its architecture, molecular composition, polydispersity, and block types as a series of parameters in the energy functional which is a nonlinear and nonlocal functional of the monomer densities and their conjugate fields. The equilibrium solutions of the SCFT energy functional correspond to the possible stable and metastable phases of the block copolymer system. They are determined by a set of the SCFT equations obtained by assigning the first variations of energy functional with respect to the density profiles and fields to zero. Finding all solutions of the SCFT equations analytically is beyond today's technology, even for the simplest *AB* diblock copolymer system. A successful alternative is to solve the SCFT equations numerically.

Numerically solving the SCFT equations requires the analysis of the property of SCFT solutions, and even the mathematical structure of the SCFT energy functional. There have been a number of numerical techniques developed to solve SCFT equations, including from the perspective of three facets – the strategy of screening initial values<sup>4-6</sup>, the numerical solver for the modified diffusion equation of chain propagators<sup>7-13</sup>, and the iterative schemes for the convergence of the equations system<sup>9,14-16</sup>. However, little work has been devoted to further analysing the mathematical structure of the SCFT even through it is well-known that the equilibrium solutions of the SCFT equations are saddle points<sup>3</sup>. Among these researches, Fredrickson and co-workers<sup>3,17,18</sup> have directly analysed the analytic structure of the field-based energy functional which does not use the mean-field approximation for incompressible polymeric systems. They utilized the Hubbard-Stratonovich transformation<sup>19</sup> to decouple the particle-particle interaction, and pointed out that, for binary component system, the physical solutions represent saddle points in which the energy functional is minimized with respect to the exchange chemical potential, and maximized with respect to the pressure potential. It is the latter field that imposes the incompressibility constraint and produces the index-1 saddle point character of the problem. The analysis of the mathematical structure of the SCFT energy functional, or more generally, of the field functional, is very useful for

the theoretical studies of polymer systems. For this reason, a series of theoretical tools have been developed including the efficient gradient-based iterative methods to solve the SCFT equations<sup>15,16</sup>, the useful technique of partial saddle-point approximation translating the saddle point problem into extreme value problem<sup>20,21</sup>, and the solving strategy for field theoretic simulation which involves numerically solving the exact partition function of polymer fluid models<sup>17,18</sup>. Due to the known information of the saddle point character, the SCFT model can be applied to the mean-field mesoscopic dynamics<sup>22,23</sup>, and the nucleation theory of ordered phases in which the saddle point problem should be turned into a minimum problem firstly, followed by the string method<sup>24</sup>.

On the other hand, in recent years, a large number of studies have been performed on the investigation of the phase behavior of multicomponent block copolymers because more chemically distinct blocks can offer opportunities to create a greater diversity of order phases and phase behaviors<sup>6,11,25-28</sup>. Because of the rapidly increasing parameters characterized the multicomponent block copolymer, the SCFT energy functional becomes more complex which also leads to a larger scale of SCFT equations system. This increases the difficulty of theoretical research and numerical simulations, and requires more theoretical analysis of the mathematical structure of the SCFT energy functional. For example, the recently developed nucleation theory of ordered phases within the SCFT using string method<sup>24</sup>, it involves converting the saddle point problem of SCFT into a minimal value problem in each iteration by a priori knowledge of saddle point character. This approach has been restricted to diblock copolymers because of lack of analysis on the saddle point property of the SCFT energy functional of multicomponent copolymer systems. In the present paper, we will analyse the analytic structure of the SCFT energy functional of multicomponent block copolymer systems based on the work of Fredrickson *et al.*. The adopted technique to use the Hubbard-Stratonovich transformation to decouple the particle-particle interaction, is not new, but it is the first time to analyse the SCFT energy functional of multicomponent (more than 2) block copolymers. The analytic structure of multicomponent block copolymer system is different from that of two-component polymer systems. In the latter system, the saddle point of physical solution is caused by the incompressibility constraint<sup>3,17,18</sup>. However, for multicomponent polymer systems, except for the incompressibility constraint, the existence of multiple non-bonded interactions will lead to high index saddle points with certain Flory-Huggins interaction parameters. In this work the influence of Flory-Huggins

interaction parameters for saddle point character of the SCFT will be detailed analysed.

The organization of the article is as follows. In Sec. II, we present the theoretical framework of the SCFT for multicomponent block copolymer system. Meanwhile the saddle point properties of the SCFT energy functional will be analysed detailedly, especially considering the influence of different Flory-Huggins interaction parameters. We also take the *ABC* triblock copolymers as a specific example to illustrate our theory in this section. In Sec. III, as an application, we will extend the gradient-based iterative method, developed in diblock copolymers, to solve the SCFT equations of multicomponent block copolymer system. Sec. IV shows the corresponding numerical results to demonstrate the availability of our developed model and numerical methods, using *ABC* star triblock copolymers model. The final section presents brief summary and some discussions on the proposed theory.

## II. THEORY

### A. Statistical particle theory

The first ingredient in the SCFT of a polymeric fluid is a mesoscopic molecular model to describe the statistical mechanics associated with the conformational states of a single polymer. In order to describe the properties of polymer chains, lots of coarse-grained polymer chain models have been developed for theoretic studies, such as continuous Gaussian chain model for flexible polymers, wormlike chain model for semiflexible or rigid-rod polymers<sup>29</sup>. For illustrative purpose, in this paper, we consider an incompressible canonical ensemble system with volume  $V$  of  $n$  flexible block copolymers. Each block copolymer has  $K$  chemically distinct subchains and  $M$  blocks (For example, *ABA* triblock copolymer has two chemically distinct subchains,  $K = 2$ , but three blocks,  $M = 3$ ). The continuous Gaussian chain model is utilized to describe macromolecular conformations. The total degree of polymerization of a block copolymer is  $N$ , and the degree of polymerization of the  $m$ -th block is  $N_m$ , then  $N = \sum_{m=1}^M N_m$ . In the continuous Gaussian model, block copolymers are represented by continuous space curves  $\mathbf{\Gamma}^j(s), j = 1, 2, \dots, n$ , where  $s \in [0, 1]$  is a normalized arc length variable measured along the chain contour. These curves are not necessary to be linear, and are also allowed the existence of star, graft shaped, and even more complex topological structure. For the  $j$ -th polymer chain,  $\mathbf{\Gamma}_\alpha^j(s)$  ( $s \in I_\alpha$ ) denotes the blocks whose monomers

belong to the same species  $\alpha, \alpha \in \{A, B, C, \dots\}$ , and  $I_\alpha$  is the interval of corresponding contour parameter.  $\mathbf{\Gamma}_\alpha^j(s)$  ( $s \in I_\alpha$ ) may be discontinuous. For example, for  $ABA$  linear triblock copolymer,  $\mathbf{\Gamma}_A^j(s)$  is used to describe the configuration of the left block  $A$  and the right block  $A$  of the  $j$ -th polymer chain.

The normalized microscopic monomer density of the type- $\alpha$  species at space position  $\mathbf{r}$  is

$$\hat{\rho}_\alpha(\mathbf{r}) = \frac{N}{\rho_0} \sum_j \int_{I_\alpha} ds \delta(\mathbf{r} - \mathbf{\Gamma}_\alpha^j(s)). \quad (1)$$

The average monomer density is  $\rho_0 = nN/V$ . Without geometry confinement or external fields, the energy functional  $H[\mathbf{\Gamma}]$ ,  $\mathbf{\Gamma} = \{\mathbf{\Gamma}^1, \mathbf{\Gamma}^2, \dots, \mathbf{\Gamma}^n\}$ , of a specific configuration state of the copolymer melt system contains harmonic stretching energy  $U_0[\mathbf{\Gamma}]$  and non-bonded interactions of between distinct monomer species  $U_1[\mathbf{\Gamma}]$ <sup>3</sup>

$$\begin{aligned} H[\mathbf{\Gamma}] &= U_0[\mathbf{\Gamma}] + U_1[\mathbf{\Gamma}], \\ \beta U_0[\mathbf{\Gamma}] &= \frac{3}{2Nb^2} \sum_{j=1}^n \int_0^1 ds \left| \frac{d\mathbf{\Gamma}^j(s)}{ds} \right|^2, \\ \beta U_1[\mathbf{\Gamma}] &= \rho_0 \int d\mathbf{r} \sum_{\alpha \neq \beta} \chi_{\alpha\beta} \hat{\rho}_\alpha(\mathbf{r}) \hat{\rho}_\beta(\mathbf{r}), \end{aligned} \quad (2)$$

where  $\chi_{\alpha\beta}$  is the Flory-Huggins interaction parameters. We here assume all statistical segments occupy the same volume  $v_0$ , and ignore differences in statistical segment length among all blocks, i.e.,  $b_\alpha = b$ . Incompressibility of the system is ensured by the delta functional in the partition function

$$Z = \int \mathcal{D}[\mathbf{\Gamma}] \delta[\hat{\rho}_+(\mathbf{r}) - 1] \times \exp(-\beta H[\mathbf{\Gamma}]), \quad (3)$$

where  $\hat{\rho}_+(\mathbf{r}) = \sum_\alpha \hat{\rho}_\alpha(\mathbf{r})$  denotes the total segment density. Thermal equilibrium occurs when the distribution function of microscopic configuration of block copolymer melts can stabilize to the Maxwell-Boltzmann distribution. In other words, the probability of finding a specific microscopic configuration  $\mathbf{\Gamma}$  is

$$P[\mathbf{\Gamma}] = \frac{\exp(-\beta H[\mathbf{\Gamma}])}{Z}, \quad (4)$$

with the configuration  $\mathbf{\Gamma}$  subjected to the incompressible condition  $\hat{\rho}_+(\mathbf{r}) = 1$ .

The essence of the saddle point (mean-field) approximation is to evaluate the most possibly observed configuration, or equivalently dominant configuration corresponding to the

global minima of the energy functional  $H[\mathbf{\Gamma}]$  subjected to the constraint of incompressibility, and neglect all the fluctuations. For the convenience of subsequent studies of evaluating the dominant configuration and approximated energy functional, we are going to transform this particle-based statistical mechanism into the statistical field theory mainly through the Hubbard-Stratonovich transformation (also named as Gaussian functional integration technique) that serves to decouple particle-particle interactions<sup>3,19</sup>.

## B. Statistical field theory

In order to use the Hubbard-Stratonovich transformation, we have to first transform the non-bonded interaction  $U_1[\mathbf{\Gamma}]$  into the normalized form

$$\beta U_1[\mathbf{\Gamma}] = -\rho_0 \int d\mathbf{r} \sum_k \zeta_k \cdot \hat{\rho}_k^2, \quad (5)$$

$\zeta_k$  is the combination of the Flory-Huggins interaction parameters  $\chi_{\alpha\beta}$  and  $\hat{\rho}_k = \sum_{\alpha} \sigma_{k\alpha} \hat{\rho}_{\alpha}$  is the linear composition of microscopic monomer densities  $\hat{\rho}_{\alpha}, \alpha \in \{A, B, C, \dots\}$ . Applying local incompressibility condition  $\hat{\rho}_+ = 1$ , or equivalently  $\hat{\rho}_A(\mathbf{r}) = 1 - \sum_{\alpha \neq A} \hat{\rho}_{\alpha}$ , to the integrand of  $U_1[\mathbf{\Gamma}]$  in (2), we have

$$\sum_{\alpha \neq \beta} \chi_{\alpha\beta} \hat{\rho}_{\alpha}(\mathbf{r}) \hat{\rho}_{\beta}(\mathbf{r}) = G[\hat{\rho}_B(\mathbf{r}), \hat{\rho}_C(\mathbf{r}) \dots] + L[\hat{\rho}_B(\mathbf{r}), \hat{\rho}_C(\mathbf{r}) \dots], \quad (6)$$

where  $G$  is a quadratic form and  $L$  is a linear composition of  $\{\hat{\rho}_B, \hat{\rho}_C, \dots\}$  (Appendix A gives the derivation process). As is well known, quadratic form  $G$  can be normalized as  $\sum_k -\zeta_k \cdot \hat{\rho}_k^2$ . Thus the non-bonded interaction energy is reduced to  $\beta U_1[\mathbf{\Gamma}] = -\rho_0 \int d\mathbf{r} \sum_k \zeta_k \cdot \hat{\rho}_k^2$  up to a constant. Because  $\int d\mathbf{r} \hat{\rho}_{\alpha}(\mathbf{r})$  is a constant unrelated to polymer configuration, adding any linear composition of  $\hat{\rho}_{\alpha}(\mathbf{r})$  to the integrand only makes a constant shift to the interacting energy  $U_1[\mathbf{\Gamma}]$ . Furthermore, because of the local incompressibility,  $\{\zeta_k, \hat{\rho}_k\}$  and  $\left\{ \zeta_k, \hat{\rho}_k = \sum_{\alpha} \tilde{\sigma}_{k\alpha} \hat{\rho}_{\alpha} = \hat{\rho}_k - \frac{1}{K} \sum_{\alpha} \sigma_{k\alpha} \hat{\rho}_+ \right\}$  describe the same interacting energy  $U_1[\mathbf{\Gamma}]$  up to a constant, but  $\hat{\rho}_k$  is orthogonal to  $\hat{\rho}_+$  for  $\sum_{\alpha} \tilde{\sigma}_{k\alpha} = 0$ . From our experience, the formula  $\left\{ \zeta_k, \hat{\rho}_k \right\}$  has a better numerical performance. There are plenty of choices for coefficients  $\zeta_k$  and linear composition  $\hat{\rho}_k$ , however, these expressions essentially describing the same non-bonded interaction  $U_1[\mathbf{\Gamma}]$  with the difference from each other being a constant.

We apply the Fourier transformation to delta functional (7)

$$\delta[\rho_+ - 1] = \int \mathcal{D}[W_+] \exp\left(-i \int d\mathbf{r} W_+ \cdot (\rho_+ - 1)\right), \quad (7)$$

and the Hubbard-Stratonovich transformation (see the Appendix B) to the “particle-based” partition function (3) and have

$$Z = \int \mathcal{D}[\mathbf{\Gamma}] \int \mathcal{D}[W_+] \int \prod_k \mathcal{D}[W_k] \exp \left\{ - \int d\mathbf{r} \sum_{\zeta_k > 0} \left( \frac{1}{4\zeta_k \rho_0} \cdot W_k^2 - W_k \cdot \hat{\rho}_k \right) - \int d\mathbf{r} \sum_{\zeta_k < 0} \left( \frac{1}{4\zeta_k \rho_0} \cdot W_k^2 - iW_k \cdot \hat{\rho}_k \right) + \int d\mathbf{r} iW_+(\hat{\rho}_+ - 1) - \beta U_0[\mathbf{\Gamma}] \right\}. \quad (8)$$

Integrating out the chain configuration  $\int \mathcal{D}[\mathbf{\Gamma}]$  leads the particle-based partition function into field-based formulism

$$Z = \int \mathcal{D}[W_+] \int \prod_k \mathcal{D}[W_k] \exp(-\beta H[\mu_+, \boldsymbol{\mu}]), \quad \boldsymbol{\mu} = (\mu_1, \mu_2, \dots), \quad (9)$$

$$H[\mu_+, \boldsymbol{\mu}] = \frac{n}{V} \int d\mathbf{r} \left[ -\mu_+ + \sum_{\zeta_k > 0} \frac{1}{4\zeta_k N} \mu_k^2 - \sum_{\zeta_k < 0} \frac{1}{4\zeta_k N} \mu_k^2 \right] - n \log Q[\boldsymbol{\omega}], \quad \boldsymbol{\omega} = (\omega_A, \omega_B, \dots), \quad (10)$$

$$\mu_+ = \frac{iN}{\rho_0} W_+, \quad \mu_k = \frac{iN}{\rho_0} W_k \quad (\text{if } \zeta_k < 0), \quad \mu_k = \frac{N}{\rho_0} W_k \quad (\text{if } \zeta_k > 0), \quad (11)$$

$$\omega_\alpha = \mu_+ - \sum_k \sigma_{k\alpha} \mu_k, \quad \alpha \in \{A, B, C, \dots\}, \quad (12)$$

where  $Q[\boldsymbol{\omega}]$  is the partition function of a single copolymer under effective mean field  $\omega_\alpha$  on type- $\alpha$  species,  $\alpha \in \{A, B, C, \dots\}$ . From the coarse-grained Gaussian continuous chain model<sup>2</sup>, the single-chain partition function  $Q$  and the monomer density  $\rho_\alpha$  can be computed through solving a set of modified diffusion equations (MDEs) of chain propagators  $q_\alpha(\mathbf{r}, s)$  and  $q_\alpha^\dagger(\mathbf{r}, s)$ ,  $s \in I_\alpha$ . These chain propagators satisfy MDEs

$$\frac{\partial}{\partial s} q_\alpha(\mathbf{r}, s) = \nabla_{\mathbf{r}}^2 q_\alpha(\mathbf{r}, s) - \omega_\alpha(\mathbf{r}) q_\alpha(\mathbf{r}, s), \quad s \in I_\alpha, \quad (13)$$

$$\frac{\partial}{\partial s} q_\alpha^\dagger(\mathbf{r}, s) = \nabla_{\mathbf{r}}^2 q_\alpha^\dagger(\mathbf{r}, s) - \omega_\alpha(\mathbf{r}) q_\alpha^\dagger(\mathbf{r}, s), \quad s \in I_\alpha. \quad (14)$$

The initial values of these MDEs are relative to the topological structure of the polymer chain<sup>3</sup>. After solving the MDEs, we can calculate the single-chain partition function

$$Q[\boldsymbol{\omega}] = \frac{1}{V} \int d\mathbf{r} q_\alpha(\mathbf{r}, s) q_\alpha^\dagger(\mathbf{r}, 1-s), \quad \forall \alpha \quad \text{and} \quad \forall s \in I_\alpha, \quad (15)$$

and the monomer density

$$\rho_\alpha = -V \left\langle \frac{\delta \log Q}{\delta \omega_\alpha} \right\rangle = \frac{1}{Q} \int_{I_\alpha} ds q_\alpha(\mathbf{r}, s) q_\alpha^\dagger(\mathbf{r}, 1-s). \quad (16)$$



### C. SCFT equations

The direct method to investigate the phase behavior of block copolymer systems is to compute the partition function (9)<sup>3</sup>. However, it is very difficult to obtain the analysis solution for such a complicated path integral. Fortunately, since the integrand is an exponential of energy functional in the complex plane, the saddle point (mean-field) approximation can be used to calculate partition function to high accuracy when concerning the most possibly configuration and ignoring the fluctuations. In the saddle point approximation, the equilibrium fields  $\mu_+^*$ ,  $\boldsymbol{\mu}^*$  dominate the functional integral (9). The field configurations are obtained by demanding that (10) be stationary with respect to fields  $\mu_+$  and  $\boldsymbol{\mu}$ , i.e.,

$$\begin{aligned} \left. \frac{\delta H(\mu_+, \boldsymbol{\mu})}{\delta \mu_+} \right|_{(\mu_+, \boldsymbol{\mu})=(\mu_+^*, \boldsymbol{\mu}^*)} &= 0, \\ \left. \frac{\delta H(\mu_+, \boldsymbol{\mu})}{\delta \mu_k} \right|_{(\mu_+, \boldsymbol{\mu})=(\mu_+^*, \boldsymbol{\mu}^*)} &= 0. \end{aligned} \quad (17)$$

Expanding the derivatives, then

$$\frac{\delta H(\mu_+^*, \boldsymbol{\mu}^*)}{\delta \mu_+^*} = \frac{n}{V} \left( \sum_{\alpha} \rho_{\alpha}(\mathbf{r}; [\mu_+^*, \boldsymbol{\mu}^*]) - 1 \right) = 0, \quad (18)$$

$$\frac{\delta H(\mu_+^*, \boldsymbol{\mu}^*)}{\delta \mu_k^*} = \frac{n}{V} \left( \frac{\mu_k^*}{2\zeta_k N} - \sum_{\alpha} \sigma_{k\alpha} \rho_{\alpha}(\mathbf{r}; [\mu_+^*, \boldsymbol{\mu}^*]) \right) = 0, \quad \zeta_k > 0, \quad (19)$$

$$\frac{\delta H(\mu_+^*, \boldsymbol{\mu}^*)}{\delta \mu_k^*} = -\frac{n}{V} \left( \frac{\mu_k^*}{2\zeta_k N} + \sum_{\alpha} \sigma_{k\alpha} \rho_{\alpha}(\mathbf{r}; [\mu_+^*, \boldsymbol{\mu}^*]) \right) = 0, \quad \zeta_k < 0. \quad (20)$$

It is well known in the polymer physics literature as SCFT equations. Having obtained the saddle point potentials  $\mu_+^*$ ,  $\boldsymbol{\mu}^*$ , one can complete the approximation by imposing  $Z \approx \exp(-\beta H[\mu_+^*, \boldsymbol{\mu}^*])$ , and obtain the value of energy functional  $\beta H[\mu_+^*, \boldsymbol{\mu}^*] = -\ln Z$ . The SCFT equations are a set of highly nonlinear system. Numerically solutions of the SCFT equations are obtained using iterative techniques. Thus analysing the mathematical structure of the energy functional is useful for prior to attempting its computation.

### D. Analytic structure of the field theory

For the purpose of implementing the saddle point approximation, it is important to get some understanding of the saddle point approximation, thereby examining the analytic

structure of the partition function (9) as well as the energy functional (10). We consider the following simple integral

$$Z(\lambda) = \int_C g(z)e^{\lambda h(z)} dz, \quad (21)$$

where  $C$  is a contour in the complex plane, and  $\lambda$  is a real positive number.  $g(z)$  and  $h(z)$ , which are independent of  $\lambda$ , are analytic functions of  $z$  in some domain of the complex plane including  $C$ . As a convenient preliminary, we introduce the functions  $u$  and  $v$  corresponding to the real part of and imaginary part of  $h(z)$  by writing

$$h(z) = u(z) + iv(z). \quad (22)$$

The problem is to find an asymptotic approximation for  $Z(\lambda)$  in the limit  $\lambda \rightarrow \infty$ . We now exploit the fact that the contour  $C$  in (21) can be deformed, by Cauchy's theorem, into other contour  $C'$  that shares the same end points, and have

$$Z(\lambda) = \int_C g(z)e^{\lambda h(z)} dz = \int_{C'} g(z)e^{\lambda h(z)} dz. \quad (23)$$

Such reexpression of  $Z$  is useful only if the integral along  $C'$  is easier than the integral along  $C$ . If  $v(z)$ , the so-called phase, is a constant along contour  $C' : v(z)|_{z \in C'} \equiv v_0$ , there are no oscillations from  $e^{i\lambda v(z)}$ . For illustrative purpose, let us use Cartesian coordinates  $x, y$  and write

$$z = z(t) = x(t) + iy(t), \quad t \in [a, b], \quad (24)$$

possibly with  $a = -\infty$  or  $b = +\infty$  or both, is a contour in the complex  $z$ -plane. Then we have

$$Z(\lambda) = e^{i\lambda v_0} \int_a^b e^{\lambda u(x(t), y(t))} u(t) dt + ie^{i\lambda v_0} \int_a^b e^{\lambda u(x(t), y(t))} v(t) dt, \quad (25)$$

where  $u(t)$  is the real part and  $v(t)$  is the imaginary part of the function  $g(z(t))z'(t)$ . We deform the path  $C$  into  $C'$  so that it passes through the saddle point  $z_0$  (i.e.,  $h'(z_0) = 0$ ), where  $u$  has its maximum value. By the Laplace method<sup>31</sup>, the major contributions to the integrals (25) come from the neighbourhoods of the points of maximum  $u(x, y)$  in the range of integration, as  $\lambda \rightarrow +\infty$ . Such a procedure is the basis of the steepest descent (or saddle point) method for the asymptotic analysis of integrals such as Eqn. (21)<sup>31</sup>.

We now return to  $Z(\lambda)$  given by (21) with the given conditions on  $g, h, \lambda$  to further observe the saddle point approximation. Firstly we show that  $z_0$  is indeed a saddle point of

$u$  (and of  $v$ ). A relative maximum of  $u$  is given by  $z_0 = x_0 + iy_0$ . Since  $u$  and  $v$  are the real and imaginary parts of  $h(z)$ , an analytic function of  $z$ , they satisfy the Cauchy-Riemann equations which are

$$u_x = v_y, \quad u_y = -v_x. \quad (26)$$

Thus

$$h'(z) = u_x + iv_x = u_x - iv_y = 0 \quad \text{when } z = z_0. \quad (27)$$

From (26),  $u$  and  $v$  are harmonic functions satisfying Laplace's equation

$$\Delta u = 0, \quad \Delta v = 0, \quad (28)$$

where  $\Delta$  is the Laplacian operator  $\partial^2/\partial x^2 + \partial^2/\partial y^2$ . By the maximum modulus theorem,  $u$  and  $v$  can not have a maximum or a minimum in the domain of analyticity of  $h(z)$ . Thus the point  $z_0$  is a saddle point of  $u$  and of  $v$ . Subsequently we point out that this specific path  $C'$  through the point of maximum  $e^{\lambda u}$  will be a path of steepest descents. Assume that  $\mathbf{s} = (dx, dy)$  is the tangential vector along the contour  $C'$ . Since  $dv(x, y) = 0$  along  $C'$ , the following equation holds

$$v_x dx + v_y dy = 0, \quad z \in C'. \quad (29)$$

By Cauchy-Riemann equation (26), we have

$$-u_y dx + u_x dy = 0. \quad (30)$$

In fact, the vector  $\boldsymbol{\tau} = (-u_y, u_x)$  is orthogonal to the  $\nabla u$ , i.e.,  $\boldsymbol{\tau} \cdot \nabla u = 0$ , thus  $\mathbf{s} \parallel \nabla u$ . That is for  $h'(z) \neq 0$ , along  $C'$  ( $C' : v(z)|_{z \in C'} = \text{const}$ ),  $u$  drops off on either side of its maximum as rapidly as possible. What is more, when we concern with saddle points of order one, that is  $h'(z_0) = 0$ ,  $h''(z_0) \neq 0$ , there exists another contour  $C''$  passing through  $z_0$  along which  $v(x, y)$  is also a constant<sup>32</sup>. The contours  $C'$  and  $C''$  are orthogonal to each other along which  $u$  changes as rapidly as possible. Assume that  $\boldsymbol{\tau} \parallel \boldsymbol{\gamma} = (-dy, dx)$ , and

$$\frac{\partial^2 u(x, y)}{\partial \mathbf{s}^2} + \frac{\partial^2 u(x, y)}{\partial \boldsymbol{\gamma}^2} = \frac{\partial^2 u(x, y)}{\partial x^2} + \frac{\partial^2 u(x, y)}{\partial y^2} = 0. \quad (31)$$

As a consequence, at the saddle point  $z_0$ ,

$$\left. \frac{d^2 u(x, y)}{d\mathbf{s}^2} \right|_{z_0} = - \left. \frac{d^2 u(x, y)}{d\boldsymbol{\gamma}^2} \right|_{z_0} < 0. \quad (32)$$

Thus the contour  $C''$  corresponds not to the steepest descent path but to the steepest ascent path since the value of  $u$  on it is such that  $u(x, y) > u(x_0, y_0)$  except at  $z_0$ . The above results are valid for multidimensional cases<sup>31</sup>. There are also a few researches for infinite-dimensional cases<sup>33-35</sup>.

We now return to the field model of multicomponent block copolymer system which is a functional integral. Strictly speaking, it is a quite challenge to find the constant phase contour  $C'$  for such a complicated infinite dimensional integral. However, for numerical purpose the fields are represented in a discrete way and the functional integral is approximated by multiply integrals of finite, but large, dimension. Thus the above heuristic discussions about the saddle point approximation are useful, at least conceptually, to determine the qualitative location and orientation of a saddle point in the complex plane.

The first thing is to verify the possibility of applying saddle point approximation to model (9). It is easily verified that the statistical weight  $\exp(-H[\mu_+, \boldsymbol{\mu}])$  is analytic functional of fields  $\mu_+(\mathbf{r})$ ,  $\boldsymbol{\mu}(\mathbf{r})$ . Thus, the deformation of integration path is conceptually possible. The original path of integration of the fields  $\mu_+(\mathbf{r})$ ,  $\boldsymbol{\mu}(\mathbf{r})$  in the partition function of (9) is along the real axis. Nevertheless, for analytic integrands  $\exp(-H[\mu_+, \boldsymbol{\mu}])$ , it is useful to deform the integration path onto a constant phase that passes through one or more saddle points  $H[\mu_+^*, \boldsymbol{\mu}^*]$  in the multi-dimensional complex plane. The phase factor  $\exp(iH_I)$  is a constant along such a contour, so that oscillations of the integrand are eliminated. A functional integral deformed onto a constant phase contour is dominated by saddle point field configurations,  $H[\mu_+^*, \boldsymbol{\mu}^*]$ , which correspond to mean-field solutions. On the constant phase contour,  $H_R$ , the real part of  $H[\mu_+, \boldsymbol{\mu}]$ , has local minima at the saddle points. The extent to which one of these saddle point field configurations dominates the integral depends on the value of a ‘‘Ginzburg parameter’’ analogous to  $\lambda$  in the above discussion. Indeed, it is straightforward to show that the coordination number  $C = (n/V)R_g^3$  is the relevant parameter<sup>3</sup>, where  $R_g$  denotes the radius of gyration of a polymer. It follows that the mean-field approximation becomes asymptotically exact for  $C \rightarrow +\infty$ . Since polymers are asymptotically ideal in the melt with  $R_g = b(N/6)^{1/2}$ , it follows that  $C \sim (\rho_0 b^3)N^{1/2}$ . Thus the saddle point approximation is accurate for concentrated solutions or melts of high-molecular-weight polymers.

The requirement that the energy functional  $H[\mu_+^*, \boldsymbol{\mu}^*]$  be real implies that  $\mu_+^*$ ,  $\mu_k^*$  ( $\eta_k < 0$ ) must be imaginary, and  $\mu_k^*$  ( $\eta_k > 0$ ) must be real, respectively. It is often convenient to

compute a purely imaginary saddle point by a relaxation scheme along the imaginary axis, which is a search direction that is orthogonal to the physical path of integration. With such a scheme, it is important to recognize that it is more than likely a descent-ascent direction for the real part of the energy functional  $H[\mu_+, \boldsymbol{\mu}]$ . Thus finding a saddle point of  $H[\mu_+, \boldsymbol{\mu}]$ , corresponding to the SCFT solution, shall be maximized with respect to the fields  $\mu_+$  and  $\mu_k$  ( $\zeta_k < 0$ ), and minimized with respect to the “exchange chemical potentials”  $\mu_k$  ( $\zeta_k > 0$ ). Thus the gradient-based iterative methods, based on the orientation of saddle points of the energy functional, can be devised to solve the SCFT equations (18)-(20).

The SCFT equations (18)-(20) have multiply solutions corresponding to more than one saddle point, which present the stable and metastable phases for polymer fluids. Inhomogeneous saddle points of interest normally require numerical iterative techniques. Within the mean-field theory, only in the vicinity of a saddle point, the orientation of the saddle point can be determined, as discussed above. Thus initial configurations shall be close to the desired saddle point in numerical computations.

The above analysis will be helpful to translate the saddle point problem into a extreme problem for multicomponent block copolymer system. For binary component incompressible polymer systems, to find saddle points, one should seek a local maximum along the exchange chemical potential  $\mu_-$ , and a local minimum along the pressure potential  $\mu_+$ <sup>3,17,18</sup>. The latter field is produced by the incompressibility constraint. Then the energy functional  $H[\mu_+, \mu_-]$  can be computed by  $H[\mu_+^*(\mu_-), \mu_-] = H[\mu_-]$  when satisfying the incompressibility condition. That is the “partial mean-field approximation”<sup>20,21</sup> which translates the saddle point problem into a minimum value problem. The “partial mean-field approximation” is useful for the nucleation theory of ordered phases<sup>24</sup> and the mesoscopic dynamics<sup>22,23</sup>. It is different from the multicomponent incompressible polymer systems. In these models, the incompressibility condition  $\delta[\hat{\rho}(\mathbf{r}) - 1]$  is also the unique constraint condition, however, the nature of the saddle point may come from the non-bond Flory-Huggins interaction parameters  $\chi_{\alpha\beta}$ . When all parameters  $\zeta_k$ , the combination of  $\chi_{\alpha\beta}$ , are positive, the SCFT solutions are local minima of  $H[\mu_+^*(\boldsymbol{\mu}), \boldsymbol{\mu}] = H[\boldsymbol{\mu}]$ . Once there exist one or more parameters such that  $\zeta_k < 0$ , the SCFT solutions are still saddle points of  $H[\mu_+^*(\boldsymbol{\mu}), \boldsymbol{\mu}]$ . Thus for multicomponent polymer systems, the original “partial mean-field approximation” cannot avoid saddle point problem. It requires the new “partial mean-field approximation”,  $H[\mu_+^*(\mu_k; \zeta_k > 0), \mu_k^*; \zeta_k < 0(\mu_k; \zeta_k > 0)]$  to translate the saddle point problem into a minimum value problem. It follows that the string

method can be applied to study the nucleation of ordered phases for multicomponent block copolymers.

Though continuous Gaussian chain model is considered here, extension to more complicated systems, for example rod-coil block copolymers and liquid crystalline side-chain copolymers with the wormlike chain model should be straight forward. Direct extensions can also be easily applied to grand canonical ensemble and compressible systems.

### E. SCFT of $ABC$ triblock copolymer melt

As an example, the SCFT of an incompressible block copolymer melt with three different chemical species, denoted by  $A$ ,  $B$ ,  $C$ , is given in this subsection. Applying the procedure proposed in Sec. II B to this system, the interaction energy of the block copolymer melt can be presented in the form

$$\begin{aligned}
U_1[\mathbf{\Gamma}] &= \rho_0 \int d\mathbf{r} [\chi_{AB}\hat{\rho}_A(\mathbf{r})\hat{\rho}_B(\mathbf{r}) + \chi_{AC}\hat{\rho}_A(\mathbf{r})\hat{\rho}_C(\mathbf{r}) + \chi_{BC}\hat{\rho}_B(\mathbf{r})\hat{\rho}_C(\mathbf{r})] \\
&= \rho_0 \int d\mathbf{r} \left\{ \frac{\Delta}{4\chi_{AC}} \hat{\rho}_B^2(\mathbf{r}) - \chi_{AC} \left[ \hat{\rho}_C(\mathbf{r}) + \frac{\chi_{AB} + \chi_{AC} - \chi_{BC}}{2\chi_{AC}} \hat{\rho}_B(\mathbf{r}) \right]^2 \right. \\
&\quad \left. + \chi_{AB}\hat{\rho}_B(\mathbf{r}) + \chi_{AC}\hat{\rho}_C(\mathbf{r}) \right\}, \tag{33}
\end{aligned}$$

where

$$\Delta = \chi_{AB}^2 + \chi_{AC}^2 + \chi_{BC}^2 - 2\chi_{AB}\chi_{AC} - 2\chi_{AB}\chi_{BC} - 2\chi_{AC}\chi_{BC}. \tag{34}$$

Omitting the linear terms, the non-bonded interaction energy becomes

$$U_1[\mathbf{\Gamma}] = \rho_0 \int d\mathbf{r} \left\{ -\zeta_1 \hat{\rho}_1^2 - \zeta_2 \hat{\rho}_2^2 \right\}, \quad \hat{\rho}_k = \sum_{\alpha} \sigma_{k\alpha} \hat{\rho}_{\alpha}, \quad k = 1, 2. \tag{35}$$

In this expression,

$$\zeta_1 = \frac{-\Delta}{4\chi_{AC}}, \quad \zeta_2 = \chi_{AC}, \tag{36}$$

and the coefficients  $\sigma_{k\alpha}$  that have been satisfied the orthogonal relation  $\hat{\rho}_+ \cdot \hat{\rho}_k = 0$  are

$$\begin{aligned}
\sigma_{1A} &= \frac{1}{3}, & \sigma_{1B} &= -\frac{2}{3}, & \sigma_{1C} &= \frac{1}{3}, \\
\sigma_{2A} &= \frac{1+\alpha}{3}, & \sigma_{2B} &= \frac{1-2\alpha}{3}, & \sigma_{2C} &= \frac{\alpha-2}{3}, & \alpha &= \frac{\chi_{AC} + \chi_{AB} - \chi_{BC}}{2\chi_{AC}}.
\end{aligned} \tag{37}$$

As discussed in the above subsection, the value of  $\zeta_k$  influences the saddle point character of the SCFT. In the following, we will analyse the expression of the SCFT for different  $\zeta_k$ .

Without loss of generality, we will assume  $\chi_{\alpha\beta} > 0$ ,  $\alpha, \beta \in \{A, B, C\}$ . The similar case of  $\chi_{\alpha\beta} < 0$  or  $\chi_{\alpha\beta} \neq 0$  can be discussed in the same way.

If  $\Delta \neq 0$ , the field-based energy functional can be written as

$$H = \frac{n}{V} \int d\mathbf{r} \left( \frac{1}{4N\zeta_1} \mu_1^2 + \frac{1}{4N\zeta_2} \mu_2^2 - \mu_+ \right) - n \log Q[\omega_A, \omega_B, \omega_C], \quad (38)$$

$$\omega_\alpha = \mu_+ - \sigma_{1\alpha} \mu_1 - \sigma_{2\alpha} \mu_2, \quad \alpha \in \{A, B, C\}. \quad (39)$$

The corresponding SCFT equations are

$$\rho_A + \rho_B + \rho_C - 1 = 0, \quad (40)$$

$$\frac{1}{2N\zeta_1} \mu_1 - \sigma_{1A} \rho_A - \sigma_{1B} \rho_B - \sigma_{1C} \rho_C = 0, \quad (41)$$

$$\frac{1}{2N\zeta_2} \mu_2 - \sigma_{2A} \rho_A - \sigma_{2B} \rho_B - \sigma_{2C} \rho_C = 0. \quad (42)$$

When  $\Delta > 0$ , the equilibrium solutions of the energy functional (38) are to be maximized with respect to the potential field  $\mu_+$  and  $\mu_1$ , and minimized with respect to another potential field  $\mu_2$ . When  $\Delta < 0$ , the equilibrium states of the energy functional (38) are the maxima along the potential field  $\mu_+$ , and minima along other potential fields  $\mu_1, \mu_2$ . When  $\Delta = 0$ , the ‘‘exchange chemical field’’  $\mu_1$  disappears. The field-based energy functional degenerates to

$$H = \frac{n}{V} \int d\mathbf{r} \left( \frac{1}{4N\zeta_2} \mu_2^2 - \mu_+ \right) - n \log Q[\omega_A, \omega_B, \omega_C], \quad (43)$$

$$\omega_\alpha = \mu_+ - \sigma_{2\alpha} \mu_2, \quad \alpha \in \{A, B, C\}. \quad (44)$$

It follows that the SCFT equations are

$$\rho_A + \rho_B + \rho_C - 1 = 0, \quad (45)$$

$$\frac{1}{2N\zeta_2} \mu_2 - \sigma_{2A} \rho_A - \sigma_{2B} \rho_B - \sigma_{2C} \rho_C = 0. \quad (46)$$

In this case, the physical solutions of the incompressible block copolymer system are saddle points in which the energy functional (43) shall be maximized along field  $\mu_+$ , and minimized along field  $\mu_2$ .

The above SCFT system is closed by combining with the single-chain partition function  $Q$  of (15), density  $\rho_\alpha$  (16) and the forward and backward propagators of MDEs (13)-(14). The

topological structure of the block copolymer chain determines the initial values of MDEs<sup>2,3</sup>. For the *ABC* linear triblock copolymer chain,

$$\begin{aligned} q_A(\mathbf{r}, 0) &= 1, & q_C^\dagger(\mathbf{r}, 0) &= 1, \\ q_B(\mathbf{r}, 0) &= q_A(\mathbf{r}, f_A), & q_B^\dagger(\mathbf{r}, 0) &= q_C^\dagger(\mathbf{r}, f_C), \\ q_C(\mathbf{r}, 0) &= q_B(\mathbf{r}, f_B), & q_A^\dagger(\mathbf{r}, 0) &= q_B^\dagger(\mathbf{r}, f_B). \end{aligned} \quad (47)$$

For the *ABC* star triblock copolymer chain,

$$q_\alpha(\mathbf{r}, 0) = 1, \quad q_\alpha^\dagger(\mathbf{r}, 0) = q_\beta(\mathbf{r}, f_\beta)q_\gamma(\mathbf{r}, f_\gamma), \quad (48)$$

where  $(\alpha\beta\gamma) \in \{(ABC), (BCA), (CAB)\}$ .

### III. GRADIENT-BASED ITERATIVE METHODS

In the preceding discussions, we have been analysed the analytic structure of the SCFT energy functional of multicomponent polymer systems, which enables us to cast light on the orientation of the saddle points corresponding to the SCFT solutions. Thus the existing gradient-based methods can be planted into multicomponent polymer systems. Essentially the SCFT equations are a set of highly nonlinear equations with multi-solutions and multi-parameters. It requires iterative techniques to solve the complicated system. For given parameters  $\chi_{\alpha\beta}$ ,  $f_\alpha$ , and fixed the calculation box, the specific iteration processes for the self-consistent systems are given in the following:

**Step 1:** Give the initial values of chemical potential fields;

**Step 2:** Solve propagators to obtain single partition function  $Q$  and density operators  $\rho_\alpha$ ;

**Step 3:** Update potential fields  $\mu_+$ ,  $\boldsymbol{\mu}$  through iterative methods;

**Step 4:** If a given convergent condition is achieved, stop iteration procedure, else goto **Step 2**.

The numerical search for equilibrium ordered structures depends on the initial conditions. A series of effective strategies have been developed for screening initial values to discover ordered patterns<sup>4-6</sup>. The subsequently numerical experiments will utilize these strategies to screen initial configurations.



Evaluating the energy functional and first derivatives of the self-consistent field models requires an efficient numerical method to solve MDEs (13) and (14) for propagators. The forth-order accurate Adams-Bashford scheme with the pseudospectral technique<sup>12</sup> is our method of choice,

$$\frac{25}{12}q^{j+1} - 4q^j + 3q^{j-1} - \frac{4}{3}q^{j-2} + \frac{1}{4}q^{j-3} = \Delta s[\nabla^2 q^{j+1} - w(4q^j - 6q^{j-1} + 4q^{j-2} - q^{j-3})]. \quad (49)$$

The initial values required to apply the multi-step scheme of (49) are obtained by using second-order operator-splitting scheme<sup>10</sup> and Richardson's extrapolation. The expressions for the derivatives of the energy functional are linearly related to density operators, which are, in turn, nonlinearly and nonlocally related to the propagators  $q$  and  $q^\dagger$  by expressions of (13) and (14). These expressions are most conveniently evaluated in real space at the collocation points of the basis functions. In particular, the composite Simpson's rule with forth-order truncation error (see Ref.<sup>36</sup>, p.134) is utilized in our numerical implementation.

Based on the proposed SCFT, we have known that at saddle points  $H[\mu_+, \boldsymbol{\mu}]$  achieves its local maxima along  $\mu_+$  and  $\mu_k$  ( $\zeta_k < 0$ ), and local minima along  $\mu_k$  ( $\zeta > 0$ ). Thus gradient-based iterative methods, such as the explicit forward Euler method, hybrid method<sup>16</sup>, and the semi-implicit method<sup>15</sup>, can be extended to update chemical potential fields of the SCFT energy functional for multicomponent block polymer systems.

**Explicit forward Euler method (EFE).** A natural approach is to introduce a fictitious "time" variable  $t$  and relax the gradient of  $H[\mu_+, \boldsymbol{\mu}]$ , which yields

$$\begin{aligned} \frac{\partial}{\partial t}\mu_+(\mathbf{r}, t) &= \frac{\delta H[\mu_+, \boldsymbol{\mu}]}{\delta \mu(\mathbf{r}, t)}, \\ \frac{\partial}{\partial t}\mu_k(\mathbf{r}, t) &= \frac{\delta H[\mu_+, \boldsymbol{\mu}]}{\delta \mu_k(\mathbf{r}, t)}, \quad \zeta_k < 0, \\ \frac{\partial}{\partial t}\mu_k(\mathbf{r}, t) &= -\frac{\delta H[\mu_+, \boldsymbol{\mu}]}{\delta \mu_k(\mathbf{r}, t)}, \quad \zeta_k > 0. \end{aligned} \quad (50)$$

A simple and useful explicit scheme is the forward Euler formula

$$\begin{aligned} \mu_+^{j+1}(\mathbf{r}) &= \mu_+^j(\mathbf{r}) + \lambda_+ \frac{\delta H[\mu_+^j, \boldsymbol{\mu}^j]}{\delta \mu_+^j(\mathbf{r})}, \\ \mu_k^{j+1}(\mathbf{r}) &= \mu_k^j(\mathbf{r}) + \lambda_k \frac{\delta H[\mu_+^j, \boldsymbol{\mu}^j]}{\delta \mu_k^j(\mathbf{r})}, \quad \zeta_k < 0, \\ \mu_k^{j+1}(\mathbf{r}) &= \mu_k^j(\mathbf{r}) - \lambda_k \frac{\delta H[\mu_+^j, \boldsymbol{\mu}^j]}{\delta \mu_k^j(\mathbf{r})}, \quad \zeta_k > 0. \end{aligned} \quad (51)$$

where iterative steps  $\lambda_+, \lambda_k > 0$ , These derivatives are computed by Eqn. (17).

**Hybrid conjugate gradient method (HCG).** The second explicit method is the hybrid scheme, firstly developed by Liang *et al.*<sup>16</sup> for flexible-semiflexible diblock copolymer system. The conjugate gradient method is normally unstable in the SCFT simulations<sup>15</sup>. However, the hybrid method combines the robustness of the steepest descent method with the efficiency of the conjugate gradient method. When minimizing an objective functional  $F[\mu]$ , the hybrid conjugate gradient method reads:

```

Let  $i = 0$ , give initial values  $\mu_0$ ,
calculate  $g_0 = \delta F[\mu]/\delta\mu$ ,  $d_0 = -g_0$ 
while  $\delta F[\mu]/\delta\mu \neq 0$  do
 $i \leftarrow i + 1$ 
choose  $\lambda_i$  to minimize  $F[\mu_i + \lambda_i d_i]$ 
 $\mu_{i+1} = \mu_i + \lambda_i d_i$ 
 $g_{i+1} = \delta F[\mu_{i+1}]/\delta\mu$ 
 $\gamma_{i+1} = (g_{i+1}^T g_{i+1}) / (g_i^T g_i)$ 
 $d_{i+1} = -g_{i+1} + \alpha_H \gamma_{i+1} d_i$ 
end while

```

In the algorithm,  $\alpha_H$  is a hybrid factor to adjust the conjugate gradient direction. If  $\alpha_H = 0$ , the hybrid scheme degenerates to steepest descent scheme. If  $\alpha_H = 1$ , it is the conjugate gradient scheme. By choosing  $0 < \alpha_H < 1$ , the hybrid method takes the advantage of the robustness of steepest descent method and the efficiency of conjugate gradient scheme. The method is not only applied to find the minima of an objective function, but also can be suitable for accomplishing the maxima of a given functional  $F[\mu]$  through first variation  $\delta F[\mu]/\delta\mu$  multiplied by  $-1$ . Therefore, the chemical potential fields  $\mu_+$  and  $\boldsymbol{\mu}$  can be all updated simultaneously by the HCG method in the light of the orientation of the saddle point of the SCFT.

**Semi-implicit method (SIM).** The third iterative method is a semi-implicit scheme, originally developed by Cenicerros and Fredrickson<sup>15</sup> for incompressible systems of homopolymer system, diblock copolymer melt and binary homopolymer blend. The pressure potential is updated using the approximated second-order variation information of  $\frac{\delta^2 H}{\delta\mu_+(\mathbf{r})\delta\mu_+(\mathbf{r}' )}$ , while the exchange chemical potential field is updated with the new field  $\mu_+$ <sup>15</sup>. The approxi-

mated second-order variation of the energy functional  $H$  with respect to  $\mu_+$  is obtained by the asymptotic expansion (or named as random phase approximation expansion<sup>3</sup>). Here we can extend the idea to multicomponent polymer systems based on the developed SCFT framework. The expression of  $\frac{\delta^2 H}{\delta\mu_+(\mathbf{r})\delta\mu_+(\mathbf{r}')}$  has been given in Appendix C. As the Ref.<sup>15</sup> recommended, we propose the semi-implicit method:

$$\hat{\mu}_+^{j+1}(\mathbf{k}) = \hat{\mu}_+^j(\mathbf{k})^j + \left( \frac{1}{\lambda_+} + \hat{G}(\mathbf{k}) \right)^{-1} \left( \frac{\widehat{\delta H[\mu_+^j, \boldsymbol{\mu}^j]}}{\delta\mu_+^j} \right)(\mathbf{k}), \quad \text{for all spectral elements } \hat{\mu}_+(\mathbf{k}), \quad (52)$$

$$\mu_k^{j+1}(\mathbf{r}) = \mu_k^j(\mathbf{r}) + \lambda_k \frac{\delta H[\mu_+^{j+1}, \boldsymbol{\mu}^j]}{\delta\mu_k^j(\mathbf{r})}, \quad \zeta_k < 0, \quad (53)$$

$$\mu_k^{j+1}(\mathbf{r}) = \mu_k^j(\mathbf{r}) - \lambda_k \frac{\delta H[\mu_+^{j+1}, \boldsymbol{\mu}^j]}{\delta\mu_k^j(\mathbf{r})}, \quad \zeta_k > 0, \quad (54)$$

where the caret denotes Fourier transform. The iterative steps  $\lambda_+, \lambda_k$  are positive numbers. In the scheme, pressure potential field  $\mu_+$  can be updated in Fourier-space conveniently by applying an FFT-inverse FFT pair with optimal computational complexity, whilst the chemical potential fields  $\mu_k$  can be updated in both real-space and Fourier space. We note that the second solutions of the MDEs (13)-(14) are required before updating potentials  $\mu_k$  in order to evaluate  $\delta H[\mu_+^{j+1}, \boldsymbol{\mu}^j]/\delta\mu_k^j(\mathbf{r})$ . This approximately doubles the computational cost per time over the explicit schemes. The step lengths  $\lambda_k$  are allowed to be larger in updating remaining chemical potential fields  $\mu_k$  with the characteristic of implicitity.

#### IV. NUMERICAL RESULTS

We will apply the developed SCFT and the extended gradient-based methods, namely EFE, HCG and SIM schemes, to  $ABC$  star triblock copolymer melts by a series of numerical experiments in three spatial dimensions. All the methods considered here have been implemented in C++ language. The cubic computational box with edge length  $D$  and periodic boundary conditions is imposed on all numerical examples. Fourier transforms in pseudo-spectral method are calculated by using the FFTW package<sup>37</sup>. The numerical experiments were run in the same computer, a Intel(R) Xeon(R) CPU E5520 @2.27 GH, memory - 24 GB, under linux. The total chain contour is discretized into  $10^2$  points (i.e.,  $\Delta s = 0.01$ ) in computing propagators  $q$  and  $q^\dagger$  with forth-order Adams-Bashford method of (49). The

uniform discretization with  $24 \times 24 \times 24$  plane waves for three-dimensional problems is used in the SCFT calculations. To measure the error, we use the  $l^\infty$  norm

$$E = \max_{\gamma} \{E_{\gamma}\}, \quad \text{where} \quad E_{\gamma} = \left\| \frac{\delta H}{\delta \mu_{\gamma}} \right\|_{l^\infty}, \quad \gamma = +, 1, 2. \quad (55)$$

From our experience, this kind of convergence criterion will produce more precise results than the relative error of the energy functional (between two consecutive iterations) at the same error tolerance. The step sizes,  $\lambda_+$ ,  $\lambda_k$ , and the hybrid factor  $\alpha_H$  in HCG are always selected as large as the stability of the methods permits and so that the error is decreased the fastest.

The value of  $\Delta$  expressed by (34) for the systems with three different chemical species influences the saddle point character of the physical relevant solutions as discussed in Sec.II E. Thus, numerical experiments for  $\Delta < 0$ ,  $\Delta = 0$ , and  $\Delta > 0$  will be implemented in the following on a case-by-case basis.

We first consider the case of  $\Delta < 0$  which is also the common used parameter range in SCFT simulations for three different chemical species systems<sup>6,28,38-41</sup>. By the analysis of the saddle point properties of SCFT solutions, to achieve the equilibrium state of *ABC* triblock copolymer model, the energy functional shall be minimized with respect to the potential fields  $\mu_1$  and  $\mu_2$ , and maximized with respect to pressure potential field  $\mu_+$ . In the first numerical experiment the Flory-Huggins interaction parameters are  $[\chi_{BC}N, \chi_{AC}N, \chi_{AB}N] = [30, 45, 30]$ . We take into account an asymmetric case  $[f_A, f_B, f_C] = [0.20, 0.70, 0.10]$ . The A15 spherical pattern of core-shell version is the target pattern. We input the space symmetric group  $Pm\bar{3}n$ <sup>5</sup> on the chemical potential field  $\mu_1$  as initial values. A cube with  $D = 7.5$  is selected as computational box.

The performance of three iterative methods, namely the error plotted against the number of iterations, is demonstrated in Fig. 1(a). The detail is presented in Tab. I. The iterations of the SIM scheme multiplied by two illustrate the feature of semi-implicit that approximately double the computational costs against the explicit schemes. Meanwhile Fig 1(b) shows the final solution of core-shell A15. These numerical results demonstrate that the gradient-based iterative schemes can reach the saddle points along the analysed directions. In particular, the HCG method takes 383 iterations to reduce the error to  $O(10^{-6})$ , SIM scheme costs 1382 iterations, and EFE approach spends 2324 iterations. In the special case the HCG scheme has the fastest rate of convergence.

TABLE I:  $ABC$  star triblock copolymer melt model:  $[\chi_{BC}N, \chi_{AC}N, \chi_{AB}N] = [30, 45, 30]$ ,  $[f_A, f_B, f_C] = [0.20, 0.70, 0.10]$ ,  $D = 7.5$ . Comparison of different iterative methods for spherical phase of A15 in core shell version.

	EFE		SIM		HCG	
Parameters	$[\lambda_+, \lambda_1, \lambda_2] = [3, 3, 3]$		$[\lambda_+, \lambda_1, \lambda_2] = [5, 5, 5]$		$[\alpha_{H,+}, \alpha_{H,1}, \alpha_{H,2}] = [0.5, 0.5, 0.5]$ $[\lambda_+, \lambda_1, \lambda_2] = [4.0, 4.0, 4.0]$	
Error	Iterations	CPU time (sec)	Iterations	CPU time (sec)	Iterations	CPU time (sec)
$E = 10^{-6}$	2324	1022	1382( $\times 2$ )	1234	864	383

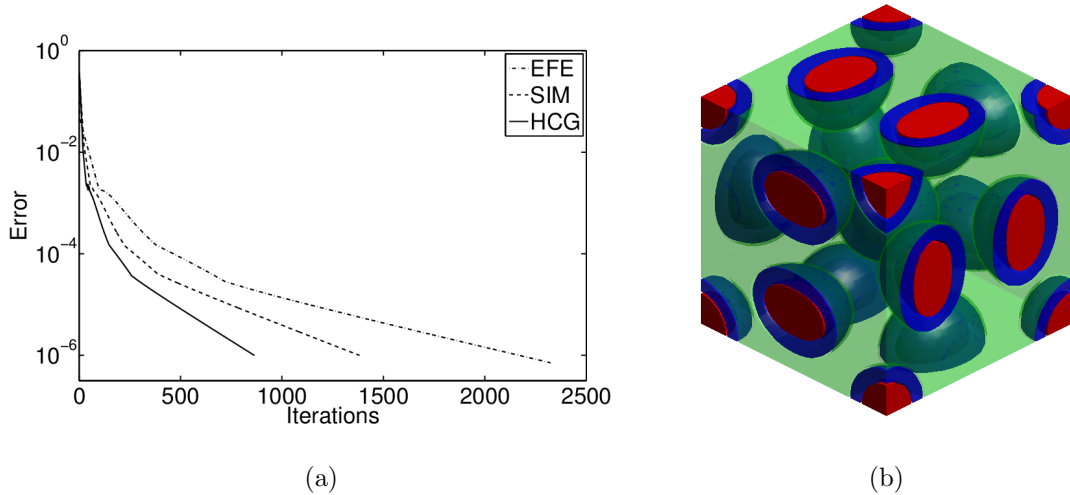


FIG. 1:  $ABC$  star triblock copolymer melt model:  $[\chi_{BC}N, \chi_{AC}N, \chi_{AB}N] = [30, 45, 30]$ ,  $[f_A, f_B, f_C] = [0.20, 0.70, 0.10]$ ,  $D = 7.5$ . (a) Comparison of the EFE scheme (dashed-dotted curve), the SIS scheme (dashed curve) and the HCG scheme (continuous curve). (b) Core-shell A15 pattern. Monomers A, B, and C are denoted by red, green, and blue colors.

The second case considered here is  $\Delta = 0$  for which  $[\chi_{BC}N, \chi_{AC}N, \chi_{AB}N] = [15, 15, 60]$ . In this case, as Sec. II E analysed, the chemical potential field of  $\mu_1$  disappears. To achieve a saddle point, one shall maximize the energy functional along  $\mu_+$ , while minimize along  $\mu_2$ .  $Fm\bar{3}m$  space group symmetry is added into the initial condition of chemical potential  $\mu_2$  to compute the objective phase of core-shell spheres in face-centered cubic (FCC) lattice. The volume fractions are  $[f_A, f_B, f_C] = [0.20, 0.63, 0.17]$ , and  $D = 4$ .

Fig. 2(a) compares the behavior of the error for the explicit forward Euler, semi-implicit, and hybrid conjugate gradient methods. In this numerical example, the error of these iterative methods has an oscillatory behavior, however, the residuals still become small against the iterations. The detailed performance of these methods at accuracy of  $10^{-6}$  is listed in Tab. II. The final morphology of FCC phase in core-shell version is shown in Fig 2(b). In this case three gradient-based iterative method can obtain the equilibrium ordered pattern in the light of the new proposed SCFT. Among these methods, the EFE method has the fewest number of iterators to reduce the error of  $O(10^{-6})$ . In particular, the EFE method is superior to the SIM and for an error of  $10^{-6}$  over 7.8 times.

TABLE II:  $ABC$  star triblock copolymer melt model:  $[\chi_{BC}N, \chi_{AC}N, \chi_{AB}N] = [15, 15, 60]$ ,  $[f_A, f_B, f_C] = [0.20, 0.63, 0.17]$ ,  $D = 4$ . Comparison of different iterative methods for FCC spherical phase in core-shell version.

	EFE		SIM		HCG	
Parameters	$[\lambda_+, \lambda_2] = [4, 4]$		$[\lambda_+, \lambda_2] = [6, 6]$		$[\alpha_{H,+}, \alpha_{H,2}] = [0.4, 0.4]$ $[\lambda_+, \lambda_2] = [2, 2]$	
Error	Iterations	CPU time (sec)	Iterations	CPU time (sec)	Iterations	CPU time (sec)
$E = 10^{-6}$	208	78	1634( $\times 2$ )	1233	298	112

As the last case we take into account  $\Delta > 0$  for  $ABC$  star triblock copolymers where the SCFT solutions become index-2 saddle points. The equilibrium states of this model shall be updating up the gradients in  $\mu_1$  and  $\mu_+$  coordinates and down the gradient in  $\mu_2$  to generate the chemical potentials. The selection of the parameters of this case is  $[\chi_{BC}N, \chi_{AC}N, \chi_{AB}N] = [52, 12, 12]$ .  $[f_A, f_B, f_C] = [0.05, 0.25, 0.70]$ . The initial values of tetragonally ordered cylinder are used for the chemical potential  $\mu_1$ . The domain size is  $D = 7$ .

Fig. 3(a) demonstrates the behavior of the error of the three iterative schemes. The final morphology of cylinders on cylinder (CoC) is shown in Fig 3(b). For this pattern, the error of these iterative methods shows an oscillatory behavior, however, the trend of the residual always declines against iterations. Tab. III presents a comparison of their performance at  $O(10^{-8})$ . The SIM and HCG methods show better numerical performance than EFE.

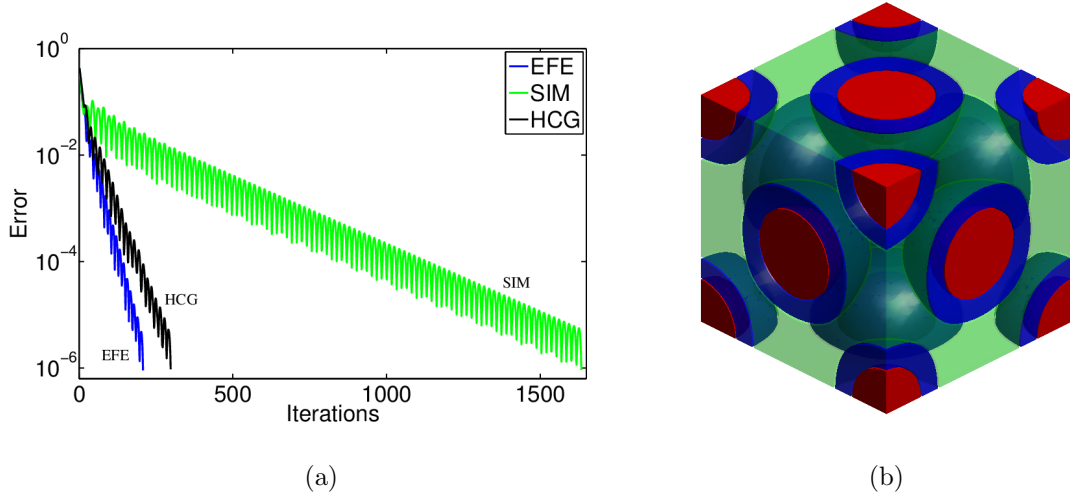


FIG. 2: ABC star triblock copolymer melt model:  $[\chi_{BC}N, \chi_{AC}N, \chi_{AB}N] = [15, 15, 60]$ ,  $[f_A, f_B, f_C] = [0.20, 0.63, 0.17]$ ,  $D = 4$ . (a) Comparison of the EFE scheme (dashed-dotted curve), the SIS scheme (dashed curve) and the HCG scheme (continuous curve). (b) Core-shell spheres in FCC lattice. Monomers A, B, and C are denoted by red, green, and blue colors.

Moreover, the SIM scheme has the fastest convergent rate, but spends more computational cost than explicit hybrid conjugate method because of the extra computational burden of the semi-implicit character. The EFE method reaches an error of  $O(10^{-8})$  after 611 seconds (1626 iterations), while SIM scheme (or HCG) accomplishes the same accuracy in just 408 seconds (371 iterations), saving nearly half of CPU time costs compared with the EFE.

TABLE III: ABC star triblock copolymer melt model:  $[\chi_{BC}N, \chi_{AC}N, \chi_{AB}N] = [52, 12, 12]$ ,  $[f_A, f_B, f_C] = [0.05, 0.25, 0.70]$ ,  $D = 7$ . Comparison of different iterative methods for CoC phase.

	EFE		SIM		HCG	
Parameters	$[\lambda_+, \lambda_1, \lambda_2] = [3, 3, 3]$		$[\lambda_+, \lambda_1, \lambda_2] = [6, 6, 6]$		$[\alpha_{H,+}, \alpha_{H,1}, \alpha_{H,2}] = [0.2, 0.2, 0.2]$ $[\lambda_+, \lambda_1, \lambda_2] = [2, 2, 2]$	
Error	Iterations	CPU time (sec)	Iterations	CPU time (sec)	Iterations	CPU time (sec)
$E = 10^{-8}$	1626	611	557( $\times 2$ )	408	998	371

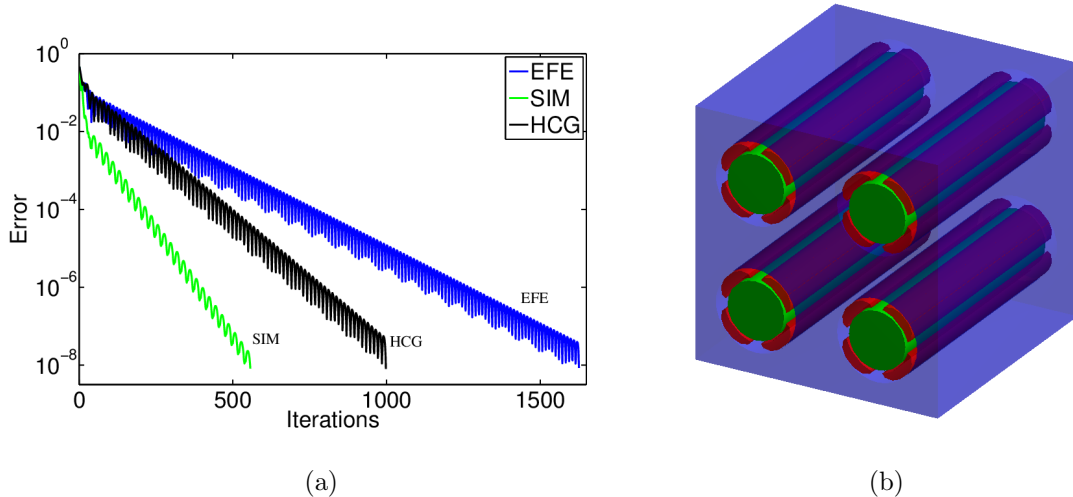


FIG. 3:  $ABC$  star triblock copolymer melt model:  $[\chi_{BC}N, \chi_{AC}N, \chi_{AB}N] = [52, 12, 12]$ ,  $[f_A, f_B, f_C] = [0.05, 0.25, 0.70]$ ,  $D = 7$ . (a) Comparison of the EFE scheme (dashed-dotted curve), the SIS scheme (dashed curve) and the HCG scheme (continuous curve). (b) the morphology of CoC pattern. Monomers A, B, and C are denoted by red, green, and blue colors.

## V. DISCUSSION AND CONCLUSIONS

We have utilized the Hubbard-Stratonovich transformation to establish the field-based theory and analysed the analytic structure of the SCFT energy functional for incompressible multicomponent block copolymer systems. Our analysis makes clear that the saddle point nature of SCFT solutions resulting from both the incompressibility constraint and the combination of the Flory-Huggins interaction parameters. Except for the incompressibility constraint, the value of  $\zeta_k$  (the combination of Flory-Huggins parameters) may give rise to high index saddle point. When  $\zeta_k < 0$ , the energy functional should be maximized with respect to  $\mu_k$ . When  $\zeta_k > 0$ , the energy functional is to be minimized with respect to  $\mu_k$ . When  $\zeta_k = 0$ , the chemical potential  $\mu_k$  disappears which reduces the number of SCFT equations. It is different from the analytic structure of the SCFT energy functional of two-component polymer systems whose saddle point character is only caused by the incompressibility condition. In this paper, we only concerns the incompressible multicomponent block copolymer systems with flexible macromolecules, however, the result can be applied to other polymer



or copolymer systems, such as blends, compressible systems and semiflexible polymers.

We believe that the analysis of the SCFT energy functional will be beneficial to many aspects of the theoretical study of multicomponent polymeric systems, such as the nucleation theory of ordered phases using the string method<sup>24</sup>, the mean-field mesoscopic dynamics. In this article we just drew our attention to the development of iterative methods to solve the SCFT equations. Based upon the analysis of the SCFT energy functional, three gradient-based iterative method, originally developed for binary-component polymer systems, have been extended to multicomponent block copolymer systems, including the EFE, HCG and SIM methods. As an application, we took *ABC* star triblock copolymer melts to demonstrate the numerical behavior of these numerical methods. Numerical experiments for  $\Delta < 0$ ,  $\Delta = 0$ , and  $\Delta > 0$  have been implemented, respectively. Numerical results indicate that these iterative methods can efficiently capture the equilibrium states along the ascent and descent paths as analysed for each case. Meanwhile we should point out that recently extended gradient-based methods are not the most effective way to solve the SCFT equations. In fact, in our numerical tests, the Anderson method<sup>14</sup>, which is a multi-step quasi-Newton method for general fixed-point problems<sup>42</sup>, performs better in the *ABC* star triblock copolymer model.

**Acknowledgements** The work is supported by the National Science Foundation of China (Grant No. 21274005 and 50930003).

## REFERENCES

- <sup>1</sup>I. W. Hamley and J. Wiley, Developments in block copolymer science and technology, Wiley Online Library, 2004.
- <sup>2</sup>M. W. Matsen, The standard Gaussian model for block copolymer melts, *Journal of Physics: Condensed Matter*, 14:R21-R47, 2002.
- <sup>3</sup>G. H. Fredrickson, The equilibrium theory of inhomogeneous polymers, Oxford University Press, USA, 2006.
- <sup>4</sup>K. Jiang, Y. Huang, and P. Zhang, Spectral method for exploring patterns of diblock copolymers, *Journal of Computational Physics*, 229:7796–7805, 2010.
- <sup>5</sup>K. Jiang, C. Wang, Y. Huang, and P. Zhang, Discovery of new metastable patterns in

- diblock copolymers, *Communications in Computational Physics*, 14:443–460, 2013.
- <sup>6</sup>W. Xu, K. Jiang, P. Zhang, and A. C. Shi, A strategy to explore stable and metastable ordered phases of block copolymers, *The Journal of Physical Chemistry B*, 117:5296–5305, 2013.
- <sup>7</sup>J. D. Vavasour and M. D. Whitmore, Self-consistent mean field theory of the microphases of diblock copolymers, *Macromolecules*, 25:5477–5486, 1992.
- <sup>8</sup>M. W. Matsen and M. Schick, Stable and unstable phases of a diblock copolymer melt, *Physical Review Letters*, 72:2660–2663, 1994.
- <sup>9</sup>F. Drolet and G. H. Fredrickson, Combinatorial screening of complex block copolymer assembly with self-consistent field theory, *Physical Review Letters*, 83:4317–4320, 1999.
- <sup>10</sup>K. Ø. Rasmussen and G. Kalosakas, Improved numerical algorithm for exploring block copolymer mesophases, *Journal of Polymer Science Part B: Polymer Physics*, 40:1777–1783, 2002.
- <sup>11</sup>Z. Guo, G. Zhang, F. Qiu, H. Zhang, Y. Yang, and A. C. Shi, Discovering ordered phases of block copolymers: New results from a generic Fourier-space approach, *Physical Review Letters*, 101:28301, 2008.
- <sup>12</sup>E. W. Cochran, C. J. Garcia-Cervera, and G. H. Fredrickson, Stability of the gyroid phase in diblock copolymers at strong segregation, *Macromolecules*, 39:2449–2451, 2006.
- <sup>13</sup>A. Ranjan, J. Qin, and D. C. Morse, Linear response and stability of ordered phases of block copolymer melts, *Macromolecules*, 41:942–954, 2008.
- <sup>14</sup>R. B. Thompson, K. Ø. Rasmussen, and T. Lookman, Improved convergence in block copolymer self-consistent field theory by Anderson mixing, *The Journal of Chemical Physics*, 120:31–34, 2004.
- <sup>15</sup>H. D. Ceniceros and G. H. Fredrickson, Numerical solution of polymer self-consistent field theory, *Multiscale Modeling and Simulation*, 2:452–474, 2004.
- <sup>16</sup>Q. Liang, K. Jiang, and P. Zhang, Efficient numerical schemes for solving self-consistent field equations of flexible-semiflexible diblock copolymers, Accepted by *Mathematical Methods in the Applied Sciences*, 2013.
- <sup>17</sup>V. Ganesan and G. H. Fredrickson, Field-theoretic polymer simulations, *Europhysics Letters*, 55:814-820, 2001.
- <sup>18</sup>G. H. Fredrickson, V. Ganesan, and F. Drolet, Field-theoretic computer simulation methods for polymers and complex fluids, *Macromolecules*, 35:16–39, 2002.

- <sup>19</sup>P. M. Chaikin and T. C. Lubensky, Principles of condensed matter physics, Cambridge University Press, 1995.
- <sup>20</sup>E. Reister, M. Müller, and K. Binder, Spinodal decomposition in a binary polymer mixture: dynamic self-consistent-field theory and Monte Carlo simulations, Physical Review E, 64:041804, 2001.
- <sup>21</sup>D. Düchs, V. Ganesan, G. H. Fredrickson, and F. Schmid, Fluctuation effects in ternary  $AB + A + B$  polymeric emulsions, Macromolecules, 36:9237–9248, 2003.
- <sup>22</sup>J. Fraaije, Dynamic density functional theory for microphase separation kinetics of block copolymer melts, The Journal of Chemical Physics, 99:9202–9212, 1993.
- <sup>23</sup>J. Fraaije, B. A. C. Van Vlimmeren, N. M. Maurits, M. Postma, O. A. Evers, C. Hoffmann, P. Altevogt, and G. Goldbeck-Wood, The dynamic mean-field density functional method and its application to the mesoscopic dynamics of quenched block copolymer melts. The Journal of Chemical Physics, 106:4260–4269, 1997.
- <sup>24</sup>X. Cheng, L. Lin, W. E, P. Zhang, and A. C. Shi, Nucleation of ordered phases in block copolymers, Physical Review Letters, 104:148301, 2010.
- <sup>25</sup>F. S. Bates, M. A. Hillmyer, T. P. Lodge, C. M. Bates, K. T. Delaney, and G. H. Fredrickson, Multiblock polymers: panacea or pandora’s box? Science, 336:434–440, 2012.
- <sup>26</sup>J. Masuda, A. Takano, Y. Nagata, A. Noro, and Y. Matsushita, Nanophase-separated synchronizing structure with parallel double periodicity from an undecablock terpolymer, Physical Review Letters, 97:98301, 2006.
- <sup>27</sup>T. H. Epps III, E. W. Cochran, T. S. Bailey, R. S. Waletzko, C. M. Hardy, and F. S. Bates, Ordered network phases in linear poly (isoprene-b-styrene-b-ethylene oxide) triblock copolymers, Macromolecules, 37:8325–8341, 2004.
- <sup>28</sup>P. Tang, F. Qiu, H. Zhang, and Y. Yang, Morphology and phase diagram of complex block copolymers:  $ABC$  star triblock copolymers, The Journal of Physical Chemistry B, 108:8434–8438, 2004.
- <sup>29</sup>M. Rubinstein and R. Colby, Polymer physics (chemistry), Oxford University Press, USA, 2003.
- <sup>30</sup>P. S. Laplace, Memoir on the probability of the causes of events, Statistical Science, 1:364–378, 1986.
- <sup>31</sup>P. D. Miller, Applied asymptotic analysis, American Mathematical Society, 2006.
- <sup>32</sup>C. M. Bender and S. A. Orszag. Advanced mathematical methods for scientists and

- engineers: Asymptotic methods and perturbation theory, Springer Verlag, 1999.
- <sup>33</sup>R. S. Ellis and J. S. Rosen, Asymptotic analysis of gaussian integrals, I: Isolated minimum points, Transactions of the American Mathematical Society, 273:447–481, 1982.
- <sup>34</sup>R. S. Ellis and J. S. Rosen, Asymptotic analysis of gaussian integrals, II: Manifold of minimum points, Communications in Mathematical Physics, 82:153–181, 1981.
- <sup>35</sup>R. S. Ellis and J. S. Rosen, Laplace’s method for gaussian integrals with an application to statistical mechanics, The Annals of Probability, 10:47–66, 1982.
- <sup>36</sup>W. H. Press, Numerical recipes: the art of scientific computing, Cambridge University Press, 2007.
- <sup>37</sup>M. Frigo and S. Johnson, Fftw: An adaptive software architecture for the FFT, ICASSP Conf. Proc., 3:1381–1384, 1998.
- <sup>38</sup>P. Tang, F. Qiu, H. Zhang, and Y. Yang, Morphology and phase diagram of complex block copolymers: *ABC* linear triblock copolymers, Physical Review E, 69:31803, 2004.
- <sup>39</sup>C. A. Tyler, J. Qin, F. S. Bates, and D. C. Morse, SCFT study of nonfrustrated *ABC* triblock copolymer melts, Macromolecules, 40:4654–4668, 2007.
- <sup>40</sup>M. Liu, W. Li, F. Qiu, and A. C. Shi, Theoretical study of phase behavior of frustrated *ABC* linear triblock copolymers, Macromolecules, 45:9522–9530, 2012.
- <sup>41</sup>W. Li and A. C. Shi. Theory of hierarchical lamellar Structures from  $A(BC)_nBA$  Multi-block Copolymers, Macromolecules, 42:811–819, 2009.
- <sup>42</sup>H. F. Walker and P. Ni, Anderson acceleration for fixed-point iterations, SIAM Journal on Numerical Analysis, 49:1715–1735, 2011.

## APPENDIX

### Appendix A: The transformation of interaction energy

Using the incompressibility condition  $\hat{\rho}_+ = \sum_{\alpha} \rho_{\alpha} = 1$ , the interaction energy of (6) in terms of congruent transformation becomes

$$\begin{aligned}
U_1[\mathbf{R}] &= \rho_0 \int d\mathbf{r} \sum_{\alpha \neq \beta} \chi_{\alpha\beta} \hat{\rho}_{\alpha}(\mathbf{r}) \hat{\rho}_{\beta}(\mathbf{r}) \\
&= \rho_0 \int d\mathbf{r} (\hat{\rho}_A, \hat{\rho}_B, \dots, \hat{\rho}_M) \begin{pmatrix} 0 & \frac{\chi_{AB}}{2} & \frac{\chi_{AC}}{2} & \dots & \frac{\chi_{AM}}{2} \\ \frac{\chi_{AB}}{2} & 0 & \frac{\chi_{BC}}{2} & \dots & \frac{\chi_{BM}}{2} \\ \vdots & \vdots & \ddots & \ddots & \vdots \\ \frac{\chi_{AM}}{2} & \frac{\chi_{BM}}{2} & \frac{\chi_{CM}}{2} & \dots & 0 \end{pmatrix} \begin{pmatrix} \hat{\rho}_A \\ \hat{\rho}_B \\ \vdots \\ \hat{\rho}_M \end{pmatrix} \\
&= \rho_0 \int d\mathbf{r} \hat{\Psi} \begin{pmatrix} 1 & 0 & 0 & \dots & 0 \\ -1 & 1 & 0 & \dots & 0 \\ \vdots & \vdots & \ddots & \ddots & \vdots \\ -1 & 0 & 0 & \dots & 0 \end{pmatrix} \begin{pmatrix} 0 & \frac{\chi_{AB}}{2} & \frac{\chi_{AC}}{2} & \dots & \frac{\chi_{AM}}{2} \\ \frac{\chi_{AB}}{2} & 0 & \frac{\chi_{BC}}{2} & \dots & \frac{\chi_{BM}}{2} \\ \vdots & \vdots & \ddots & \ddots & \vdots \\ \frac{\chi_{AM}}{2} & \frac{\chi_{BM}}{2} & \frac{\chi_{CM}}{2} & \dots & 0 \end{pmatrix} \begin{pmatrix} 1 & -1 & -1 & \dots & -1 \\ 0 & 1 & 0 & \dots & 0 \\ \vdots & \vdots & \ddots & \ddots & \vdots \\ 0 & 0 & 0 & \dots & 0 \end{pmatrix} \hat{\Psi}^T \\
&= \rho_0 \int d\mathbf{r} \hat{\Psi} \cdot S_1 \cdot \hat{\Psi}^T \\
&= \rho_0 \int d\mathbf{r} \hat{\Psi} \cdot S_2 \cdot \hat{\Psi}^T + C(\chi_{\alpha\beta}, \rho_0, N_{\alpha}, V), \\
&= -\rho_0 \int d\mathbf{r} \sum_{k=1}^{M-1} \zeta_k \left( \sum_{\alpha=1}^M \sigma_{k\alpha} \hat{\rho}_{\alpha} \right)^2 + C(\chi_{\alpha\beta}, \rho_0, N_{\alpha}, V), \\
&= -\rho_0 \int d\mathbf{r} \sum_{k=1}^{M-1} \zeta_k \hat{\rho}_k^2 + C(\chi_{\alpha\beta}, \rho_0, N_{\alpha}, V) \\
&\stackrel{\Delta}{=} G[\hat{\rho}_B(\mathbf{r}), \hat{\rho}_C(\mathbf{r}) \dots] + L[\hat{\rho}_B(\mathbf{r}), \hat{\rho}_C(\mathbf{r}) \dots],
\end{aligned} \tag{A1}$$

where

$$S_1 = \begin{pmatrix} 0 & \frac{\chi_{AB}}{2} & \frac{\chi_{AC}}{2} & \cdots & \frac{\chi_{AM}}{2} \\ \frac{\chi_{AB}}{2} & -\chi_{AB} & \cdots & \cdots & \\ \frac{\chi_{AC}}{2} & & -\chi_{AC} & (s_{ij}) & \vdots \\ \vdots & (s_{ji}) & \ddots & \ddots & \vdots \\ \frac{\chi_{AM}}{2} & & \cdots & \cdots & -\chi_{AM} \end{pmatrix}, \quad S_2 = \begin{pmatrix} 0 & 0 & 0 & \cdots & 0 \\ 0 & -\chi_{AB} & & \cdots & \\ 0 & & -\chi_{AC} & (s_{ij}) & \vdots \\ \vdots & (s_{ji}) & \ddots & \ddots & \vdots \\ 0 & & \cdots & \cdots & -\chi_{AM} \end{pmatrix},$$

$$s_{ij} = s_{ji} = \frac{\chi_{ij} - \chi_{1i} - \chi_{1j}}{2}, \quad j > i > 2.$$

$\hat{\Psi} = (\hat{\rho}_+, \hat{\rho}_B, \dots, \hat{\rho}_M)$ ,  $\zeta_k$  are the compositions of  $\chi_{\alpha\beta}$ ,  $\hat{\rho}_k = \sum_{\alpha=1}^M \sigma_{k\alpha} \hat{\rho}_\alpha$ ,  $\sigma_{k\alpha}$  are constants. The constant term  $C$  just represents a constant shift in energy functional and dose not influence the configuration of the system. We here utilize the incompressibility condition to eliminate the  $\hat{\rho}_A$  in the transformation of interaction energy. There are also other options, such as eliminating  $\hat{\rho}_\alpha$  ( $\alpha \neq A$ ) to translate  $U_1[\mathbf{R}]$ . The difference is only a constant, but it also does not influence the configuration of the system.

## Appendix B: Gaussian functional integrals

The following Gaussian functional integrals using in the Hubbard-Stratonovich transformation can be also found in Refs. <sup>3,19</sup>.

$$\frac{\int Df \exp[-(1/2) \int dx \int dx' f(x)A(x, x')f(x') + \int dx J(x)f(x)]}{\int Df \exp[-(1/2) \int dx \int dx' f(x)A(x, x')J(x')]} = \exp\left(\frac{1}{2} \int dx \int dx' J(x)A^{-1}(x, x')J(x')\right), \quad (\text{B1})$$

$$\frac{\int Df \exp[-(1/2) \int dx \int dx' f(x)A(x, x')f(x') + i \int dx J(x)f(x)]}{\int Df \exp[-(1/2) \int dx \int dx' f(x)A(x, x')J(x')]} = \exp\left(-\frac{1}{2} \int dx \int dx' J(x)A^{-1}(x, x')J(x')\right), \quad (\text{B2})$$

where  $A(x, x')$  is assumed to be real, symmetric, and positive definite. The functional inverse of  $A$ ,  $A^{-1}$ , is defined by

$$\int dx' A(x, x')A^{-1}(x', x'') = \delta(x - x''). \quad (\text{B3})$$

When these formulas are applied to interacting particle models in classical statistical physics.  $J$  represents a microscopic density operator, and  $A$  is a pair potential function. The function  $f$  is an auxiliary potential that serves to decouple particle-particle interactions.

### Appendix C: The second-order variation of $H$ with respect to $\mu_+$

In this Appendix, we use the random phase approximated expansion<sup>3</sup> to obtain the approximate expression of the second-order variation of the SCFT energy functional  $H$  with respect to  $\mu_+$ . We firstly consider the  $ABC$  triblock linear copolymer systems. A particularly useful perturbation expansion can be derived when the potential field  $\omega_\alpha$ , where  $\alpha = A, B, C$  has inhomogeneities that are weak in amplitude. We expand potential fields  $\omega_\alpha$  as

$$\omega_\alpha(\mathbf{r}) = \omega_{0,\alpha} + \varepsilon\omega_{1,\alpha}, \quad \omega_{0,\alpha} = \frac{1}{V} \int d\mathbf{r} \omega_\alpha(\mathbf{r}), \quad (\text{C1})$$

$\varepsilon$  is a small parameter  $\varepsilon \ll 1$ . Let's translate propagator  $q(\mathbf{r}, s)$  into

$$q(\mathbf{r}, s) = p(\mathbf{r}, s) \exp\left(-\int_0^s d\tau \omega_0(\mathbf{r}, s)\right), \quad (\text{C2})$$

which leads to

$$\frac{\partial p}{\partial s} = \nabla^2 p(\mathbf{r}, s) - \varepsilon\omega_1 p(\mathbf{r}, s), \quad p(\mathbf{r}, 0) = 1. \quad (\text{C3})$$

A weak inhomogeneity expansion can be developed by assuming that  $p(\mathbf{r}, s)$  can be expressed as

$$p(\mathbf{r}, s) \sim \sum_{j=1}^{\infty} \varepsilon^j p^{(j)}(\mathbf{r}, s). \quad (\text{C4})$$

Using these expressions, single chain partition function  $Q$  (see Eqn.(15)) can be written as

$$Q = \hat{q}(\mathbf{0}, 1) = \exp\left(-\int_0^1 d\tau \omega_0(\mathbf{r}, \tau)\right) \left[ p^{(0)}(\mathbf{r}, 1) + \varepsilon p^{(1)}(\mathbf{r}, 1) + \varepsilon^2 p^{(2)}(\mathbf{r}, 1) + o(\varepsilon^3) \right]. \quad (\text{C5})$$

In particular,

$$p^{(0)}(\mathbf{r}, 1) = 1, \quad (\text{C6})$$

$$\begin{aligned} \hat{p}^{(1)}(\mathbf{k}, s) &= \frac{\hat{\omega}_{1,A}(\mathbf{k})}{\mathbf{k}^2} (1 - e^{\mathbf{k}^2 f_A}) e^{-\mathbf{k}^2 s} + \frac{\hat{\omega}_{1,B}(\mathbf{k})}{\mathbf{k}^2} (1 - e^{\mathbf{k}^2 f_B}) e^{-\mathbf{k}^2 (s-f_A)} \\ &\quad + \frac{\hat{\omega}_{1,C}(\mathbf{k})}{\mathbf{k}^2} (1 - e^{\mathbf{k}^2 (s-f_A-f_B)}) e^{-\mathbf{k}^2 (s-f_A-f_B)}, \end{aligned} \quad (\text{C7})$$

$$\begin{aligned} \hat{p}^{(2)}(\mathbf{0}, 1) &= \frac{1}{2} \int d\mathbf{k}_1 \hat{\omega}_{1,C}(-\mathbf{k}_1) \hat{\omega}_{1,C}(\mathbf{k}_1) \hat{g}_{CC} + \frac{1}{2} \int d\mathbf{k}_1 \hat{\omega}_{1,C}(-\mathbf{k}_1) \hat{\omega}_{1,A}(\mathbf{k}_1) \hat{g}_{AC} \\ &\quad + \frac{1}{2} \int d\mathbf{k}_1 \hat{\omega}_{1,C}(-\mathbf{k}_1) \hat{\omega}_{1,B}(\mathbf{k}_1) \hat{g}_{BC} + \frac{1}{2} \int d\mathbf{k}_1 \hat{\omega}_{1,B}(-\mathbf{k}_1) \hat{\omega}_{1,B}(\mathbf{k}_1) \hat{g}_{BB} \\ &\quad + \frac{1}{2} \int d\mathbf{k}_1 \hat{\omega}_{1,A}(-\mathbf{k}_1) \hat{\omega}_{1,A}(\mathbf{k}_1) \hat{g}_{AA} + \frac{1}{2} \int d\mathbf{k}_1 \hat{\omega}_{1,B}(-\mathbf{k}_1) \hat{\omega}_{1,A}(\mathbf{k}_1) \hat{g}_{AB}, \end{aligned} \quad (\text{C8})$$

where

$$\begin{aligned}
\hat{g}(\mathbf{k}, s) &= \frac{2}{\mathbf{k}^2} \left( e^{-\mathbf{k}s} + \mathbf{k}s - 1 \right), \\
\hat{g}_{AA} &= \hat{g}(\mathbf{k}^2, f_A), \\
\hat{g}_{BB} &= \hat{g}(\mathbf{k}^2, f_B), \\
\hat{g}_{AB} &= \hat{g}(\mathbf{k}^2, f_A + f_B) - \hat{g}(\mathbf{k}^2, f_B) - \hat{g}(\mathbf{k}^2, f_A), \\
\hat{g}_{CC} &= \hat{g}(\mathbf{k}^2, f_C), \\
\hat{g}_{AC} &= \hat{g}(\mathbf{k}^2, 1) - \hat{g}(\mathbf{k}^2, f_A + f_B) - \hat{g}(\mathbf{k}^2, 1 - f_A) + \hat{g}(\mathbf{k}^2, f_B), \\
\hat{g}_{BC} &= \hat{g}(\mathbf{k}^2, 1 - f_A) - \hat{g}(\mathbf{k}^2, f_B) - \hat{g}(\mathbf{k}^2, f_C).
\end{aligned} \tag{C9}$$

Therefore,

$$\begin{aligned}
Q \sim \exp \left( - \int_0^1 d\tau \omega_0(\mathbf{r}, \tau) \right) & \left[ 1 - \varepsilon \hat{\omega}_{1,A}(0) f_A - \varepsilon \hat{\omega}_{1,B}(0) f_B - \varepsilon \hat{\omega}_{1,C}(0) f_C + \frac{\varepsilon^2}{2} \int d\mathbf{k} \hat{\omega}_{1,C}(-\mathbf{k}) \hat{\omega}_{1,C}(\mathbf{k}) \hat{g}_{CC} \right. \\
& + \frac{\varepsilon^2}{2} \int d\mathbf{k} \hat{\omega}_{1,C}(-\mathbf{k}) \hat{\omega}_{1,A}(\mathbf{k}) \hat{g}_{AC} + \frac{\varepsilon^2}{2} \int d\mathbf{k} \hat{\omega}_{1,C}(-\mathbf{k}) \hat{\omega}_{1,B}(\mathbf{k}) \hat{g}_{BC} + \frac{\varepsilon^2}{2} \int d\mathbf{k} \hat{\omega}_{1,B}(-\mathbf{k}) \hat{\omega}_{1,B}(\mathbf{k}) \hat{g}_{BB} \\
& \left. + \frac{\varepsilon^2}{2} \int d\mathbf{k} \hat{\omega}_{1,A}(-\mathbf{k}) \hat{\omega}_{1,A}(\mathbf{k}) \hat{g}_{AA} + \frac{\varepsilon^2}{2} \int d\mathbf{k} \hat{\omega}_{1,B}(-\mathbf{k}) \hat{\omega}_{1,A}(\mathbf{k}) \hat{g}_{AB} \right].
\end{aligned}$$

Note that  $\hat{\omega}_{\alpha,1}(0) = 0$ , we have

$$\begin{aligned}
\frac{\partial \log Q}{\partial \hat{\omega}_A(-\mathbf{k})} &= \frac{1}{Q} \frac{\partial Q}{\partial \hat{\omega}_A(-\mathbf{k})} \approx \hat{\mu}_+ \left( \frac{1}{2} \hat{g}_{AC} + \hat{g}_{AA} + \frac{1}{2} \hat{g}_{AB} \right) - \hat{\mu}_1 \left( \frac{a_{13}}{2} \hat{g}_{AC} + a_{11} \hat{g}_{AA} + \frac{a_{12}}{2} \hat{g}_{AB} \right) \\
& - \mu_2 \left( \frac{a_{23}}{2} \hat{g}_{AC} + a_{21} \hat{g}_{AA} + \frac{a_{22}}{2} \hat{g}_{AB} \right),
\end{aligned} \tag{C10}$$

$$\begin{aligned}
\frac{\partial \log Q}{\partial \hat{\omega}_B(-\mathbf{k})} &= \frac{1}{Q} \frac{\partial Q}{\partial \hat{\omega}_B(-\mathbf{k})} \approx \hat{\mu}_+ \left( \frac{1}{2} \hat{g}_{BC} + \hat{g}_{BB} + \frac{1}{2} \hat{g}_{AB} \right) - \hat{\mu}_1 \left( \frac{a_{13}}{2} \hat{g}_{BC} + a_{12} \hat{g}_{BB} + \frac{a_{11}}{2} \hat{g}_{AB} \right) \\
& - \mu_2 \left( \frac{a_{23}}{2} \hat{g}_{BC} + a_{22} \hat{g}_{BB} + \frac{a_{21}}{2} \hat{g}_{AB} \right),
\end{aligned} \tag{C11}$$

$$\begin{aligned}
\frac{\partial \log Q}{\partial \hat{\omega}_C(-\mathbf{k})} &= \frac{1}{Q} \frac{\partial Q}{\partial \hat{\omega}_C(-\mathbf{k})} \approx \hat{\mu}_+ \left( \frac{1}{2} \hat{g}_{AC} + \hat{g}_{CC} + \frac{1}{2} \hat{g}_{BC} \right) - \hat{\mu}_1 \left( \frac{a_{11}}{2} \hat{g}_{AC} + a_{13} \hat{g}_{CC} + \frac{a_{12}}{2} \hat{g}_{BC} \right) \\
& - \hat{\mu}_2 \left( \frac{a_{21}}{2} \hat{g}_{AC} + a_{23} \hat{g}_{CC} + \frac{a_{22}}{2} \hat{g}_{BC} \right).
\end{aligned} \tag{C12}$$

Summing them up,

$$\begin{aligned}
\frac{\partial \log Q}{\partial \hat{\mu}_+(-\mathbf{k})} &= \frac{\partial \log Q}{\partial \hat{\omega}_A(-\mathbf{k})} + \frac{\partial \log Q}{\partial \hat{\omega}_B(-\mathbf{k})} + \frac{\partial \log Q}{\partial \hat{\omega}_C(-\mathbf{k})} \\
& \approx \hat{\mu}_+(\mathbf{k}) (\hat{g}_{AA} + \hat{g}_{BB} + \hat{g}_{CC} + \hat{g}_{AB} + \hat{g}_{AC} + \hat{g}_{BC}) + o(\hat{\mu}_1) + o(\hat{\mu}_2).
\end{aligned} \tag{C13}$$

We also note

$$\hat{g}_{AA} + \hat{g}_{BB} + \hat{g}_{CC} + \hat{g}_{AB} + \hat{g}_{AC} + \hat{g}_{BC} = \hat{g}(\mathbf{k}^2, 1) = \hat{G}(\mathbf{k}), \tag{C14}$$



and the energy functional of  $ABC$  triblock copolymers in Fourier-space is

$$H = -\hat{\mu}_+(\mathbf{0}) + \frac{1}{4N\beta_1} \sum_{\mathbf{k}} \hat{\mu}_1(\mathbf{k}) \hat{\mu}_1(-\mathbf{k}) + \frac{1}{4N\beta_2} \sum_{\mathbf{k}} \hat{\mu}_2(\mathbf{k}) \hat{\mu}_2(-\mathbf{k}) - \log \hat{q}(\mathbf{0}, 1). \quad (\text{C15})$$

Thus

$$\widehat{\left( \frac{\delta^2 H}{\delta \mu_+^2} \right)}(\mathbf{k}) = -\frac{2}{\mathbf{k}^4} (e^{-\mathbf{k}^2} + \mathbf{k}^2 - 1) \triangleq -\hat{G}(\mathbf{k}), \quad (\text{C16})$$

where the caret denotes Fourier transform. In fact, the above result is hold for general linear multi-block copolymers by the same derivative process.

Following the above derivative process, for general nonlinear polymer chain, the approximation second-order variation of  $H$  with respect to  $\mu_+$  in Fourier space is

$$\widehat{\left( \frac{\delta^2 H}{\delta \mu_+^2} \right)}(\mathbf{k}) \approx -\sum_{\alpha} \hat{g}_{\alpha\alpha}(\mathbf{k}^2) \triangleq -\hat{G}(\mathbf{k}), \quad (\text{C17})$$

where  $\hat{g}_{\alpha\alpha}(\mathbf{k}) = 2(e^{-\mathbf{k}f_{\alpha}} + \mathbf{k}f_{\alpha} - 1)/\mathbf{k}^2$  is the familiar Debye function<sup>3</sup>,  $\alpha$  denotes the  $\alpha$ -th species.